

# On the rapid demise of Lyman- $\alpha$ emitters at redshift $z \gtrsim 7$ due to the increasing incidence of optically thick absorption systems

James S. Bolton<sup>1,2</sup> & Martin G. Haehnelt<sup>3</sup>

<sup>1</sup> *School of Physics and Astronomy, University of Nottingham, University Park, Nottingham, NG7 2RD*

<sup>2</sup> *School of Physics, University of Melbourne, Parkville, VIC 3010, Australia*

<sup>3</sup> *Kavli Institute for Cosmology and Institute of Astronomy, Madingley Road, Cambridge, CB3 0HA*

14 October 2018

## ABSTRACT

A variety of independent observational studies have now reported a significant decline in the fraction of Lyman-break galaxies which exhibit Ly $\alpha$  emission over the redshift interval  $z = 6-7$ . In combination with the strong damping wing extending redward of Ly $\alpha$  in the spectrum of the bright  $z = 7.085$  quasar ULAS 1120+0641, this has strengthened suggestions that the hydrogen in the intergalactic medium (IGM) is still substantially neutral at  $z \sim 7$ . Current theoretical models imply H I fractions as large as 40–90 per cent may be required to explain these data assuming there is no intrinsic evolution in the Ly $\alpha$  emitter population. We propose that such large neutral fractions are not necessary. Based on a hydrodynamical simulation which reproduces the absorption spectra of high-redshift ( $z \sim 6-7$ ) quasars, we demonstrate that the opacity of the intervening IGM redward of rest-frame Ly $\alpha$  can rise rapidly in average regions of the Universe simply because of the increasing incidence of absorption systems which are optically thick to Lyman continuum photons as the tail-end of reionisation is approached. Our simulations suggest these data do not require a large change in the IGM neutral fraction by several tens of per cent from  $z = 6-7$ , but may instead be indicative of the rapid decrease in the typical mean free path for ionising photons expected during the final stages of reionisation.

**Key words:** dark ages, reionisation, first stars - galaxies: high-redshift - intergalactic medium - quasars: absorption lines.

## 1 INTRODUCTION

The opacity observed blueward of rest frame Ly $\alpha$  in the spectra of distant quasars rises toward higher redshifts (Fan et al. 2006; Becker et al. 2007), indicating the fraction of neutral hydrogen in the intergalactic medium (IGM) is small but increasing with lookback time. This observation, coupled with the Thomson optical depth measured from cosmic microwave background data (Komatsu et al. 2011), suggests that an extended epoch of hydrogen reionisation was ending by  $z \sim 6-7$ . Reaching further into the epoch of reionisation – when intergalactic hydrogen is still substantially neutral – is difficult, but Ly $\alpha$  selected galaxies may offer one promising route to probing somewhat deeper into this distant era (Miralda-Escudé & Rees 1998; Haiman 2002). The increasing H I content in the IGM at  $z > 6$  produces a Ly $\alpha$  damping wing which can extend redward of a galaxy’s Ly $\alpha$  emission line. The damping wing reduces the visibility of the Ly $\alpha$  emission (Miralda-Escudé 1998), and the num-

ber of Ly $\alpha$  emitting galaxies (LAEs) observed in flux-limited surveys will thus decrease as the ambient H I fraction rises with increasing redshift (Haiman & Spaans 1999).

The resonant nature of the Ly $\alpha$  transmission unfortunately complicates this simple picture. Source clustering (Furlanetto et al. 2006), dust (Hansen & Oh 2006; Dayal et al. 2011), and resonant Ly $\alpha$  scattering within the sources themselves – which is sensitive to both the H I content and gas velocities (Santos 2004; Dijkstra & Wyithe 2010) – all impact on the visibility of Ly $\alpha$  emission. The complex resonant radiative transfer within the galaxies often leads to substantial line redshifts of several hundred  $\text{km s}^{-1}$  which can significantly enhance the visibility of LAEs when the surrounding IGM is still substantially neutral (Dijkstra et al. 2011; Laursen et al. 2011; Zheng et al. 2011; Barnes et al. 2011; Jeesson-Daniel et al. 2012).

Recently, however, a significant decrease in the trans-

mission of Ly $\alpha$  photons from high redshift galaxies has been found between  $z = 6-7$ , (Stark et al. 2010; Pentericci et al. 2011; Hayes et al. 2011; Ono et al. 2012; Schenker et al. 2012; Curtis-Lake et al. 2012). This result is based on the rapid decline in the fraction of Lyman break galaxies (LBGs) which exhibit Ly $\alpha$  emission – a quantity which is (in principle) less susceptible than the LAE luminosity function (e.g. Malhotra & Rhoads 2004; Kashikawa et al. 2006; Hu et al. 2010) to observational selection effects and intrinsic evolution in the LAE population. Based on comparisons to existing numerical simulations and semi-numerical models of reionisation, the reported rapid decrease in the transmission of Ly $\alpha$  emission at  $z \sim 6-7$  may be interpreted as a rapid change in the volume-averaged neutral fraction (by several tens of percent) over a rather short redshift interval (Pentericci et al. 2011; Schenker et al. 2012; Ono et al. 2012).

Such a rapid change in the neutral fraction is, however, at odds with the rather low ionising emissivity suggested by the Ly $\alpha$  forest data at  $z = 5-6$  (Bolton & Haehnelt 2007b) which appears to imply a much slower evolution of the neutral fraction. Theoretical reionisation models matching the Ly $\alpha$  forest data (e.g. Ciardi et al. 2012; Kuhlen & Faucher-Giguère 2012; Jensen et al. 2012) therefore have considerable difficulty in explaining the rather large neutral fractions ( $\sim 40-90$  per cent) that have been inferred from the recent LAE/LBG observations at  $z \sim 7$ . Alternative explanations which – either individually or in combination – might allow for a more modest change in the IGM neutral fraction include an increase in the escape fraction of ionising photons, or an increase in the interstellar dust content of the galaxies toward higher redshift (see Forero-Romero et al. 2012 for further discussion of these points).

In this paper, we shall argue that one other clue to this puzzle is provided by the quasar ULAS J1120+0641 at  $z = 7.085$ , recently discovered by the UKIRT Infrared Deep Sky Survey (UKIDSS, Lawrence et al. 2007). The spectrum of ULAS J1120+0641 exhibits a strong Ly $\alpha$  damping wing extending redward of the quasar Ly $\alpha$  emission line (Mortlock et al. 2011) – exactly what is needed to suppress the generally redshifted (relative to the systemic redshift of the galaxy) emission of LAEs. Theoretical models predict that the regions surrounding rare, bright quasars are amongst the first to reionise (e.g. Furlanetto et al. 2004; Iliiev et al. 2006; Trac & Cen 2007; Zahn et al. 2007; McQuinn et al. 2007b). If the environment around ULAS J1120+0641 is typical of quasar host galaxies at  $z > 7$ , the significantly weaker ionising radiation field expected around even the brightest LAEs implies the impact of the red Ly $\alpha$  damping wing on LAE visibility should be even stronger.

Bolton et al. (2011) used high resolution simulations of Ly $\alpha$  absorption to demonstrate that unless a proximate damped Ly $\alpha$  absorber lies within  $\sim 5$  pMpc of the quasar, a volume averaged H I fraction of at least  $\langle f_{\text{HI}} \rangle_{\text{v}} = 0.1$  is required to reproduce the damping wing observed around ULAS J1120+0641. In this work we show that an H I fraction of around 10 per cent could also explain the rapid evolution of the LAEs – obviating the need for H I fractions as large as 40–90 per cent. The difference in the inferred neutral fraction is due to the inclusion of small-

scale ( $\sim 20$  pkpc), optically thick absorptions systems which remain unresolved in large-scale ( $\gtrsim 100$  cMpc) reionisation simulations. On including these systems the Ly $\alpha$  opacity up to a few hundred  $\text{km s}^{-1}$  redward of rest frame Ly $\alpha$  rises more rapidly with H I fraction than usually predicted. As we shall demonstrate, this is because the intervening Ly $\alpha$  opacity of the IGM at the end of hydrogen reionisation is strongly affected by the increasing size of these systems, which naturally occurs as the metagalactic photo-ionisation rate decreases. A more modest neutral fraction of  $\sim 10$  per cent is much easier to reconcile with the fact that quasar absorption spectra at  $z \simeq 6$  appear to indicate that the IGM is highly ionised only 180 Myr later (Fan et al. 2006; Wyithe et al. 2008, but see also Mesinger 2010).

We begin our analysis in Section 2, where we describe our modelling of the IGM Ly $\alpha$  opacity and the procedure we adopt for incorporating self-shielded gas into a hydrodynamical simulation. In Section 3 the properties of the optically thick absorbers in the simulations are discussed in more detail. We explore the implications of these absorption systems for the visibility of Ly $\alpha$  emission from galaxies in Section 4, and in Section 5 we conclude. We assume the cosmological parameters  $\Omega_{\text{m}} = 0.26$ ,  $\Omega_{\Lambda} = 0.74$ ,  $\Omega_{\text{b}} h^2 = 0.023$ ,  $h = 0.72$  and a helium mass fraction of  $Y = 0.24$  throughout. Comoving and proper distances are denoted by using the prefixes “c” and “p”, respectively.

## 2 NUMERICAL SIMULATIONS OF THE IGM

### 2.1 Hydrodynamical model

We model the IGM using a high-resolution hydrodynamical simulation performed with the parallel Tree-SPH code GADGET-3, last described in Springel (2005). The simulation employs a box size of  $10h^{-1}$  cMpc, a gas particle mass of  $9.2 \times 10^4 h^{-1} M_{\odot}$  and a gravitational softening length of  $0.65h^{-1}$  ckpc. The gas is reionised instantaneously by a uniform, optically thin ionising background at  $z = 9$  based on the Haardt & Madau (2001) galaxies and quasars emission model. Although we subsequently recompute the ionisation state of the gas, this means the IGM density field at  $z \leq 9$  is already Jeans smoothed by the increased gas pressure following photo-heating (e.g. Pawlik et al. 2009). This simulation was previously used to model the Ly $\alpha$  opacity in the near-zone of the high-redshift quasar ULAS J1120+0641 at  $z = 7.085$  (Bolton et al. 2011). In this work we use an output at  $z = 7$ .

The initial equilibrium ionisation state of the gas is set by a spatially uniform ionising background. We do not model the patchy ionisation state of the IGM by following the radiative transfer of ionising photons emitted by individual sources. We will, however, estimate the effect of a central source on the ionisation state of the IGM later in our analysis. A box size of  $10h^{-1}$  cMpc is in any case too small to correctly capture the large scale topology of the reionisation process. Instead, the high mass resolution of the simulation allows us to incorporate the small-scale structures responsible for optically thick absorption systems. These absorption systems are expected to define the edge of ionised bubbles (Crociani et al. 2011), regulate the mean free path at overlap (Miralda-Escudé et al. 2000; Gnedin & Fan 2006;

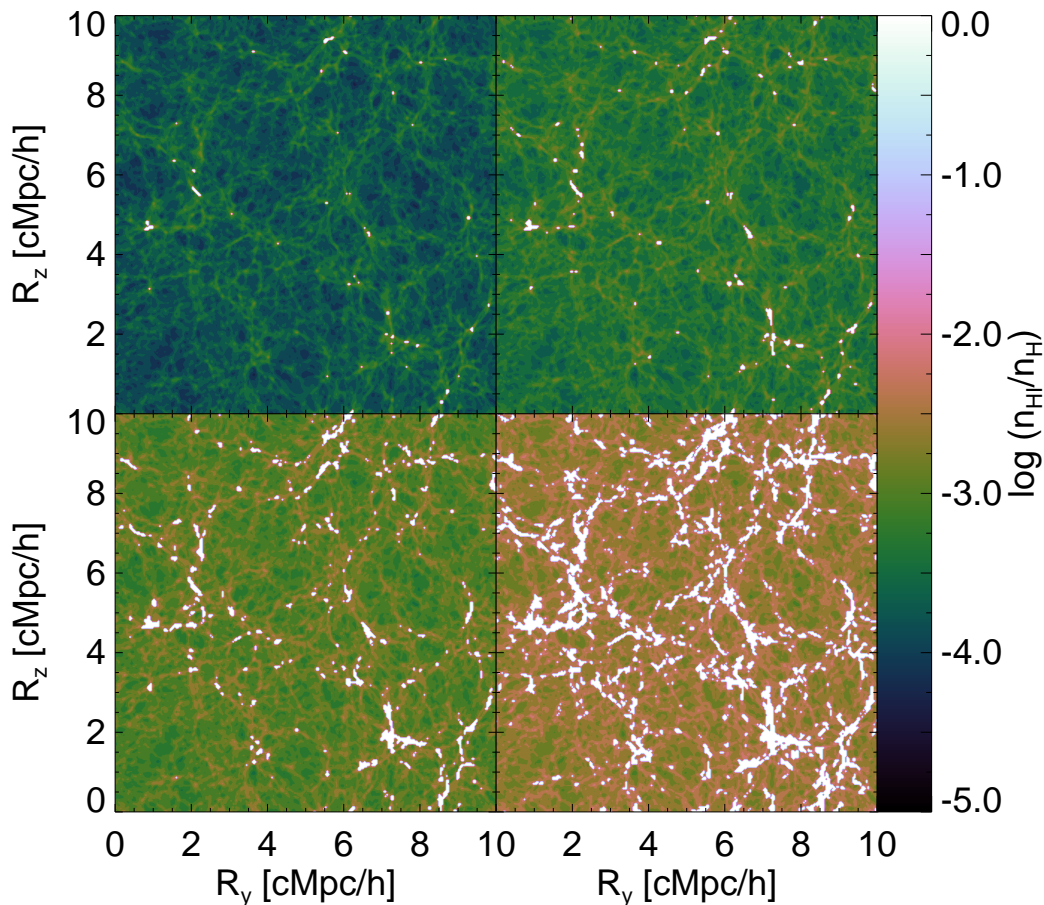


**Figure 1.** Slices midway ( $R_x = 5h^{-1}$  cMpc, with width  $\Delta R_x = 39h^{-1}$  ckpc) through the hydrodynamical simulation volume at  $z = 7$  displaying the spatial distribution of the neutral hydrogen fraction,  $n_{\text{HI}}/n_{\text{H}}$ , for four different background photo-ionisation rates. A self-shielding prescription (see Eq. 1) has been used in all four cases. Fully neutral self-shielded regions, which trace the highest density regions in the simulation, are shaded white. Anti-clockwise from top left,  $\log(\Gamma_{\text{HI}}/\text{s}^{-1}) = -12.8, -13.6, -14.0$  and  $-13.2$ .

McQuinn et al. 2011) and delay the latter stages of reionisation (Ciardi et al. 2006; Alvarez & Abel 2012). These systems remain unresolved in most large-scale reionisation simulations (but see Choudhury et al. 2009; Crociani et al. 2011; Alvarez & Abel 2012 for recent “semi-numerical” approaches, and Gnedin & Fan 2006; Kohler & Gnedin 2007; McQuinn et al. 2011; Altay et al. 2011 for smaller simulations which resolve self-shielded systems) and are therefore often not considered when estimating the impact of intergalactic Ly $\alpha$  absorption on the visibility of LAEs.

## 2.2 Modelling optically thick absorption systems

In order to include optically thick absorbers in our model, following Schaye (2001) we use a simple, physically motivated prescription to assign a density threshold above which gas remains self-shielded, which we briefly summarise here (see also Miralda-Escudé et al. 2000; Furlanetto & Oh 2005). Assuming that the typical size of an H I absorber is the Jeans scale and adopting the case-A recombination coefficient for ionised hydrogen (Abel et al. 1997), the overden-

sity at which an H I absorber begins to self-shield may be approximated as:

$$\Delta_{\text{ss}} = 36 \Gamma_{-12}^{2/3} T_4^{2/15} \left( \frac{\mu}{0.61} \right)^{1/3} \left( \frac{f_e}{1.08} \right)^{-2/3} \left( \frac{1+z}{8} \right)^{-3}, \quad (1)$$

where  $\Gamma_{-12} = \Gamma_{\text{HI}}/10^{-12} \text{s}^{-1}$  is the background photo-ionisation rate,  $T_4 = T/10^4 \text{K}$  is the gas temperature,  $\mu$  is the mean molecular weight and  $f_e = n_e/n_{\text{H}}$  is the free electron fraction with respect to hydrogen. Absorbers at this density threshold have a characteristic size

$$L_{\text{ss}} = 8.7 \text{pkpc} \Gamma_{-12}^{-1/3} T_4^{13/30} \left( \frac{\mu}{0.61} \right)^{-2/3} \left( \frac{f_e}{1.08} \right)^{1/3}. \quad (2)$$

The fiducial values adopted for  $f_e$  and  $\mu$  correspond to a plasma of ionised hydrogen and singly ionised helium. Note that helium is not expected to be doubly ionised until  $z \sim 3$  (e.g. Furlanetto & Oh 2008; McQuinn et al. 2009). Comparison to radiative transfer calculations indicate this simple prescription recovers the density at which intergalactic gas self-shields to within a factor of two at  $z = 6$  (McQuinn et al. 2011).

We shall consider four different values for the background photo-ionisation rate in this work:  $\log(\Gamma_{\text{HI}}/\text{s}^{-1}) =$

**Table 1.** The four background photo-ionisation rates used in this work. The resulting volume weighted neutral hydrogen fractions (which include the contribution from self-shielded gas) are summarised in the second column.

$\log(\Gamma_{\text{HI}}/\text{s}^{-1})$	$\langle f_{\text{HI}} \rangle_{\text{V}}$
-12.8	$2.7 \times 10^{-3}$
-13.2	$9.2 \times 10^{-3}$
-13.6	$3.2 \times 10^{-2}$
-14.0	$1.1 \times 10^{-1}$

-12.8, -13.2, -13.6 and -14.0. These are summarised in Table 1 along with the corresponding volume weighted H I fractions. This range is chosen so that the largest value is comparable to recent photo-ionisation rate measurements from the Ly $\alpha$  forest at  $z = 6$  (Wyithe & Bolton 2011; Calverley et al. 2011). The lowest value produces a volume averaged H I fraction of around ten per cent (with  $\Delta_{\text{ss}} \sim 2$ ), and thus approaches the regime where this self-shielding prescription ceases to provide an adequate description<sup>1</sup> of the spatial distribution of H I in the IGM.

Figure 1 displays the resulting distribution of neutral hydrogen in a two dimensional slice of the simulation. The self-shielding threshold given by Eq. (1) is computed self-consistently using the temperatures and densities from the hydrodynamical simulation. Neutral hydrogen (shaded white) traces the densest parts of the cosmic-web, and fills a progressively larger fraction of the simulation volume as the amplitude of the ionising background is lowered.

### 2.3 Extracting line-of-sight quantities

We use these neutral hydrogen distributions as the starting point for constructing mock Ly $\alpha$  absorption spectra. Sight-lines are extracted parallel to the box boundaries in three directions around the 100 most massive dark matter haloes in the simulation at  $z = 7$ . These halo sight-lines are spliced together with sight-lines drawn randomly from the periodic volume to form a total of 300 continuous skewers through the density, peculiar velocity and temperature field of the hydrodynamical simulation. The skewers have a total length of 12.5 pMpc, ranging from 8330 km s<sup>-1</sup> to -2084 km s<sup>-1</sup> around the halo position. The Ly $\alpha$  optical depth along each of the sight-lines is then computed following a standard procedure, see e.g. eq. (15) in Bolton & Haehnelt (2007a). In the rest of our analysis, all quantities will be estimated from these 300 sight-lines.

We note, however, that the most massive dark matter halo in the simulation volume at  $z = 7$  has a mass  $M_{\text{dm}} = 9.0 \times 10^9 M_{\odot}$ . In comparison, Ouchi et al. (2010) infer an average dark matter host halo mass of  $10^{10}$ – $10^{11} M_{\odot}$  from the clustering of LAEs with  $L_{\text{Ly}\alpha} > 2.5 \times 10^{42}$  erg s<sup>-1</sup> at  $z = 6.6$ . Our simulation is therefore too small to correctly

<sup>1</sup> In other words, when the IGM is no longer in the “post-overlap” stage of reionisation (cf. Gnedin 2000) and neutral gas also resides in underdense regions far from ionising sources. This self-shielding model only applies to what is sometimes referred to as the final “outside-in” stages of reionisation (e.g. Miralda-Escudé et al. 2000; Choudhury et al. 2009; Finlator et al. 2009).

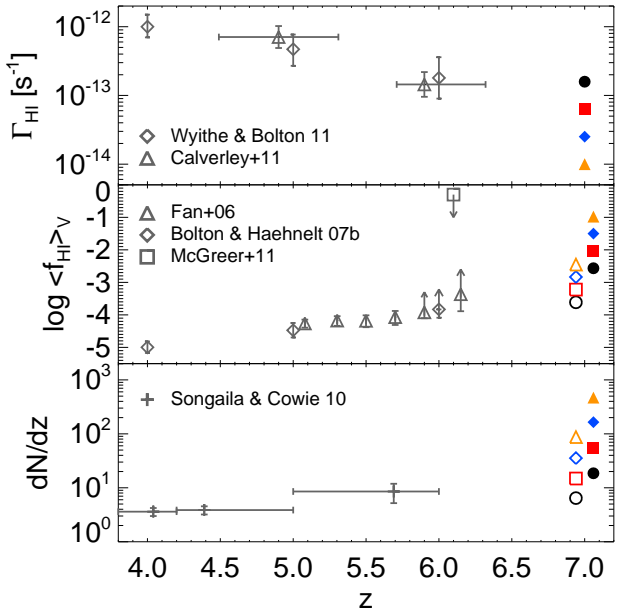


**Figure 2.** *Top:* comparison of the four photo-ionisation rates assumed in this work (filled symbols at  $z = 7$ ) with observational constraints at  $z \leq 6$  from the Ly $\alpha$  forest opacity (Wyithe & Bolton 2011) and the line-of-sight proximity effect (Calverley et al. 2011). *Middle:* the filled symbols (offset from  $z = 7$  for clarity) display the corresponding volume averaged H I fraction. The open symbols show the H I fraction which results if self-shielding (see Eq. 1) is not included. Observational constraints at  $z \leq 6.1$  are from IGM Ly $\alpha$  absorption measurements (Fan et al. 2006; Bolton & Haehnelt 2007b; McGreer et al. 2011). *Bottom:* the number density of absorption systems with  $10^{17.2} \leq N_{\text{HI}}/\text{cm}^{-2} \leq 10^{20.0}$  per unit redshift. The filled (open) symbols at  $z = 7$  again show the model predictions including (excluding) gas which is self-shielded from the ionising background. The data points with error bars display the number density of absorbers per unit redshift measured by Songaila & Cowie (2010) at  $z < 6$ , rescaled to match the cosmological parameters assumed in this work.

sample typical LAE host haloes while simultaneously resolving the small-scale structure of the IGM, so in what follows we will underestimate the impact of the more extended gas overdensities and/or stronger inflows expected around larger haloes on the visibility of the Ly $\alpha$  emitters. However, both of these effects will tend to make the impact of Ly $\alpha$  absorption on the visibility of the Ly $\alpha$  emitters stronger, rather than weaker, serving to strengthen our main conclusion that modest H I fractions may explain the observed LAE fraction at  $z = 7$ .

### 3 PROPERTIES OF THE OPTICALLY THICK ABSORBERS

It is instructive to first make contact with observations by comparing our simulation results at  $z = 7$  to constraints from the IGM at  $z \leq 6$ . The upper panel in Figure 2 displays the four photo-ionisation rates used in Figure 1. The filled symbols in the middle panel display the corresponding volume averaged H I fractions predicted by these models.

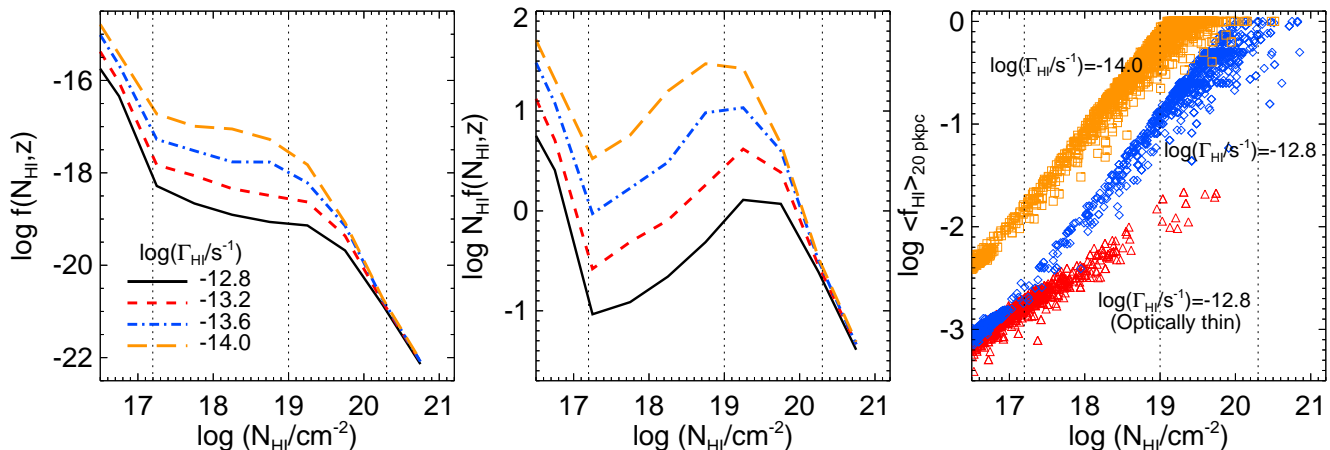


**Figure 3.** *Left:* the column density distribution function predicted at  $z = 7$  for the four different background ionisation rates indicated on the plot. The vertical dotted lines demarcate the column density thresholds by which we define LLSs ( $10^{17.2} \leq N_{\text{HI}}/\text{cm}^{-2} < 10^{19.0}$ ), super-LLSs ( $10^{19.0} \leq N_{\text{HI}}/\text{cm}^{-2} < 10^{20.3}$ ) and DLAs ( $N_{\text{HI}} \geq 10^{20.3} \text{ cm}^{-2}$ ). *Middle:* as for left panel but now displaying  $\log N_{\text{HI}} f(N_{\text{HI}})$ . *Right:* scatter plots of absorber H I fractions against H I column density for the largest and smallest of the ionisation rates assumed. The red triangles show the results obtained when self-shielding is ignored for  $\log(\Gamma_{\text{HI}}/\text{s}^{-1}) = -12.8$  only.

The lowest H I fraction is consistent with only weak evolution from the lower observational limit at  $z = 6$ , whereas smaller photo-ionisation rates result in a stronger increase in the H I fraction toward  $z = 7$ . Note these H I fractions are higher than the values expected if self-shielding were ignored – this is demonstrated by the open symbols at  $z \sim 7$ , which display the H I fraction computed from our simulated sight-lines without the self-shielding prescription given by Eq. (1) (i.e. assuming a uniform, optically thin ionising background).

The bottom panel of Figure 2 displays the resulting number density of absorption systems with column<sup>2</sup> densities  $10^{17.2} \leq N_{\text{HI}}/\text{cm}^{-2} \leq 10^{20.0}$ , along with the recent observational measurements presented by Songaila & Cowie (2010) at  $z \leq 6$ . The filled (open) symbols again display the results including (excluding) self-shielding. Lowering the amplitude of the H I ionising background significantly increases the incidence of these absorption systems. This increase is more pronounced in the models incorporating self-shielding, with a factor of  $\sim 25$  increase in the number density of absorbers per unit redshift from  $\log(\Gamma_{\text{HI}}/\text{s}^{-1}) = -12.8$  to  $-14.0$ .

The absorber properties are displayed in more detail in Figure 3, where the left panel displays the H I column density distribution functions (CDDFs) obtained from the simulations. The CDDF follows the conventional definition:

$$f(N_{\text{HI}}, z) = \frac{\partial^2 N}{\partial z \partial N_{\text{HI}}} \frac{H(z)}{H_0(1+z)^2}. \quad (3)$$

Including self-shielding increases the number of optically thick absorbers, flattening the otherwise power-law column density distribution at  $10^{17.2} \leq N_{\text{HI}}/\text{cm}^{-2} \leq 10^{19.2}$ . A similar flattening of the CDDF is inferred from observations at  $z \sim 3.7$  (Prochaska et al. 2010), and it has also

been noted in many other theoretical models (Katz et al. 1996; Zheng & Miralda-Escudé 2002; Nagamine et al. 2010; McQuinn et al. 2011; Altay et al. 2011). The distributions converge at  $N_{\text{HI}} \sim 10^{20} \text{ cm}^{-2}$ , indicating the highest column density systems (damped Ly $\alpha$  absorbers with  $N_{\text{HI}} \geq 10^{20.3} \text{ cm}^{-2}$ ) remain largely insensitive to changes in the background photo-ionisation rate by virtue of their high gas density, at least for  $\Gamma_{\text{HI}} \leq 10^{-12.8} \text{ s}^{-1}$ . The middle panel in Figure 3 displays  $N_{\text{HI}} f(N_{\text{HI}})$ , which indicates which optically thick systems comprise the bulk of the H I opacity. When self-shielding is included, it is absorption systems with  $N_{\text{HI}} \sim 10^{18.5} - 10^{19.5} \text{ cm}^{-2}$  which dominate.

Finally, the ionisation state of the optically thick absorbers are displayed in the right panel of Figure 3 (see also figure 5 of McQuinn et al. 2011). The blue diamonds and orange squares show the average H I fraction against column density for  $\log(\Gamma_{\text{HI}}/\text{s}^{-1}) = -12.8$  and  $-14.0$ , respectively. As the photo-ionisation rate is lowered, the density threshold for self-shielding is reduced (since  $\Delta_{\text{ss}} \propto \Gamma_{-12}^{2/3}$ ) and the size and incidence rate of optically thick absorption systems (i.e.  $N_{\text{HI}} > \sigma_{\text{HI}}^{-1} = 10^{17.2} \text{ cm}^{-2}$ , where  $\sigma_{\text{HI}}$  is the H I photo-ionisation cross-section at the Lyman limit) increases. The self-shielded regions first extend into the outer parts of galactic haloes and then into the filaments defining the cosmic web (e.g. Figure 1). For comparison, the red triangles display the results obtained for  $\log(\Gamma_{\text{HI}}/\text{s}^{-1}) = -12.8$  when ignoring self-shielding. Absorbers with the same  $N_{\text{HI}}$  have larger H I fractions when self-shielding is included, implying these must correspond to regions of lower gas density relative to the optically thin case. As we shall now demonstrate, it is this rapid increase in the incidence of optically thick absorption systems with increasing neutral fraction at the tail-end of reionisation which is primarily responsible for strengthening the red Ly $\alpha$  damping wing in our simulations.

<sup>2</sup> Column densities are estimated by integrating the density field over a scale of 20 pkpc; this choice is motivated by Eq. (2), which yields  $L_{\text{ss}} \simeq 16\text{--}40$  pkpc for the range of photo-ionisation rates considered here.

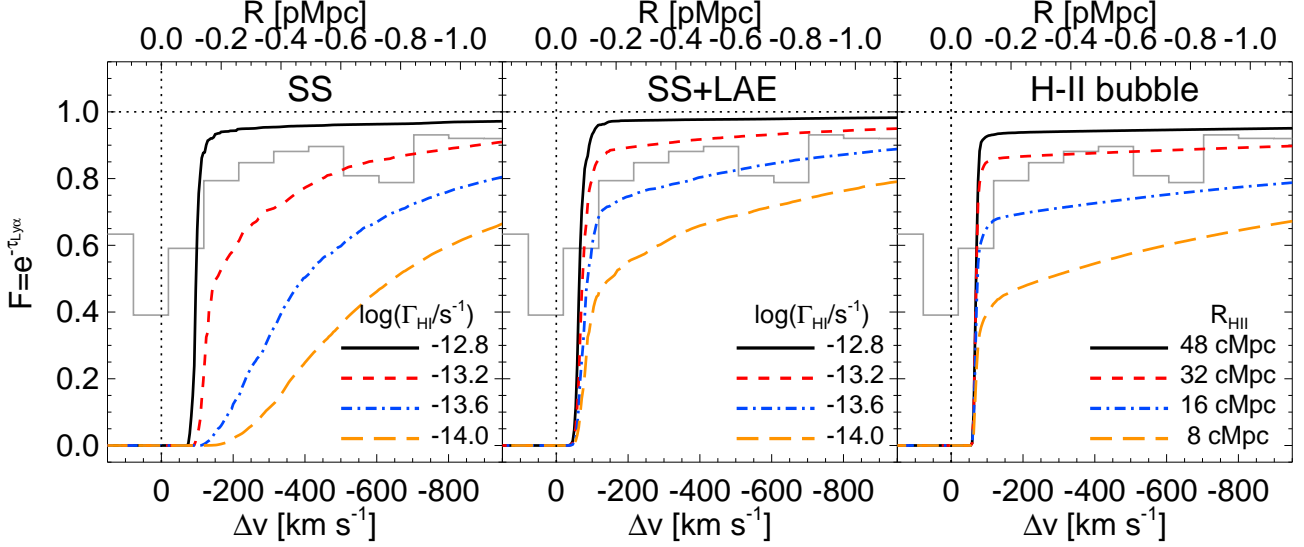


**Figure 4.** The median Ly $\alpha$  transmission redward of the rest frame Ly $\alpha$  transition (at  $\Delta v = 0 \text{ km s}^{-1}$ ) obtained from an ensemble of 300 simulated sight-lines. Each panel displays a different intergalactic Ly $\alpha$  absorption model. The four continuous curves in each panel display the transmission profile for different background ionisation rates as indicated. The binned grey line displays the observed transmitted fraction around the  $z = 7.085$  quasar ULAS J1120+0641 with an estimated  $\dot{N}_{\text{ion}} = 1.3 \times 10^{57} \text{ s}^{-1}$ . *Left:* model which includes self-shielded (SS) gas, but ignores the influence of a central ionising source. *Centre:* as for left panel, but now each sight-line includes the photo-ionisation rate from an LAE with  $L_{\text{Ly}\alpha} = 5 \times 10^{42} \text{ erg s}^{-1}$  which emits ionising photons at a rate  $\dot{N}_{\text{ion}} = 1.1 \times 10^{53} \text{ s}^{-1}$ . *Right:* a model which neglects optically thick systems, and instead models the ionisation state of the IGM as an ionised bubble with radius  $R_{\text{HII}}$  embedded in an otherwise fully neutral IGM. The H II bubble sizes are as indicated on the plot. Note this case is shown to emulate results from existing models in the literature only.

## 4 IMPLICATIONS FOR LAE VISIBILITY

### 4.1 Photo-ionisation by a central source

We now turn to the main result in this paper; estimating the impact of the increasing incidence of optically thick absorbers on the visibility of LAEs. Before proceeding further, however, we also allow for the possible effect of ionising radiation from a central source in our models (i.e. the Ly $\alpha$  emitter under observation). Ionising radiation from the LAE itself can reduce the incidence of proximate self-shielded gas and therefore weaken the Ly $\alpha$  damping wing.

We model the possible effect of the LAE as follows. Firstly, we compute the emission rate of ionising photons into the IGM,  $\dot{N}_{\text{ion}} [\text{s}^{-1}]$ , by an LAE with observed Ly $\alpha$  luminosity  $L_{\text{Ly}\alpha}$  assuming case-B recombination:

$$\dot{N}_{\text{ion}} = \frac{3 L_{\text{Ly}\alpha}}{2 h_{\text{P}} \nu_{\alpha}} \frac{f_{\text{esc}}}{(1 - f_{\text{esc}}) f_{\alpha}}. \quad (4)$$

Here the energy of a Ly $\alpha$  photon is  $h_{\text{P}} \nu_{\alpha} = 10.2 \text{ eV}$ , and  $f_{\text{esc}}$  and  $f_{\alpha}$  are the escape fractions of Lyman continuum and Ly $\alpha$  photons into the IGM. In this work we follow Dijkstra et al. (2007) and assume  $f_{\alpha} = 1$ , such that  $L_{\text{Ly}\alpha} = f_{\alpha} L_{\text{Ly}\alpha}^{\text{intr}}$  yields the Ly $\alpha$  luminosity uncorrected for dust. We adopt  $L_{\text{Ly}\alpha} = 5 \times 10^{42} \text{ erg s}^{-1}$  based on the typical Ly $\alpha$  luminosities measured in recent observations of  $z \sim 7$  LAEs (e.g. Pentericci et al. 2011). We assume a Lyman continuum escape fraction of  $f_{\text{esc}} = 0.2$ , which yields  $\dot{N}_{\text{ion}} = 1.1 \times 10^{53} \text{ s}^{-1}$ . The Lyman continuum escape fraction is highly uncertain. A value  $\gtrsim 20$  per cent is required at  $z \simeq 6$  if the observed Lyman break galaxy population is to reproduce ionising background constraints from the Ly $\alpha$  forest (Bolton & Haehnelt 2007b; Shull et al. 2012;

Finkelstein et al. 2012), but as we will discuss in more detail in Section 4.4 the relation between Ly $\alpha$  emission and the escape of ionising radiation may not be straightforward.

In the models with a central ionising source we then assume the total photo-ionisation rate to be the sum of the LAE contribution and the metagalactic background rate:

$$\Gamma_{\text{HI}}^{\text{tot}}(R) = \sigma_{\text{HI}} \frac{\dot{N}_{\text{ion}}}{4\pi R^2} \frac{\beta}{\beta + 3} + \Gamma_{\text{HI}}, \quad (5)$$

where we have assumed a power law spectral energy distribution for the ionising radiation from the LAE,  $L_{\nu} \propto \nu^{-\beta}$ , with  $\beta = 3$  (cf. Leitherer et al. 1999). Note that we have ignored (i) the finite lifetime of the LAE, effectively assuming the ionising radiation propagates instantaneously along the line-of-sight (ii) the intervening H I opacity between self-shielded systems and (iii) assumed the LAE luminosity is constant. All three assumptions will maximise the impact of ionising radiation from the LAE on the surrounding neutral hydrogen. In what follows we therefore consider this as a limiting case and bracket other possibilities by additionally computing the Ly $\alpha$  damping wing when the LAE is ignored. We do not explicitly account for the possible clustering of ionising sources around the LAE in addition to the range of background photo-ionisation rates we already consider. As we shall demonstrate in the next section, larger background photo-ionisation rates weaken the red Ly $\alpha$  damping wing by raising the density threshold at which gas self-shields.

### 4.2 The red Ly $\alpha$ damping wing

Figure 4 displays the median IGM Ly $\alpha$  transmission profile obtained from the 300 simulated sight-lines – each panel

corresponds to a different IGM absorption model. Note that when computing the transmission profiles we have ignored the contribution of all gas within 20 pkpc of the centre of the LAE host halo to both the Lyman continuum and Ly $\alpha$  opacity. We do not model the complex radiative transfer within the host galaxy's interstellar medium, and account for the absorption by this material with the parameters  $f_{\text{esc}}$  and  $f_{\alpha}$  instead.

The left panel shows the transmission profile predicted by our simulations without photo-ionisation by the LAE. A strong damping wing profile is produced, even for photo-ionisation rates that correspond to H I fractions as low as  $\sim 3$  per cent (blue dot-dashed curve). This is due to the presence of high column density LLS or damped Ly $\alpha$  absorption systems within  $\sim 1$  pMpc of the LAE host halo (at  $\Delta v = 0 \text{ km s}^{-1}$ ). For comparison, the grey binned line in all panels displays the transmission profile of the  $z = 7.085$  quasar ULAS J1120+0641 (Mortlock et al. 2011); a strong damping wing extends redwards of systemic Ly $\alpha$  despite the expected quasar proximity effect and the fact that the biased regions where bright quasars form should reionise earlier than on average. This implies that if similar ionisation conditions hold around bright LAEs at  $z = 7$ , an even stronger red damping wing may result.

The central panel instead shows the damping wings for our models including ionising emission from an LAE. The source dominates the total photo-ionisation rate (i.e. produces more than 50 per cent of the total) within  $\sim 0.5$  pMpc. The incidence of proximate, self-shielded systems within this radius is therefore significantly reduced, and the Ly $\alpha$  damping wing is consequently weakened. On the other hand, recall that the typical halo mass in our simulations is rather small (see Section 2.3). We therefore likely underestimate the abundance of proximate optically thick systems and this effect may be somewhat less important. The convergence of the transmission profiles at  $F = 0$  (close to  $\Delta v = -50 \text{ km s}^{-1}$ ) is due to peculiar velocities arising from gravitational infall around the haloes. We have verified that ignoring peculiar motions produces profiles which converge at  $\Delta v = 0 \text{ km s}^{-1}$  instead. Note that in the left panel of Figure 4, where emission from a central LAE is excluded, this convergence is less prominent. This is because absorption line cores from proximate absorbers in addition to the Ly $\alpha$  damping wing can extend redward of systemic Ly $\alpha$ ; this occurs more frequently as the photo-ionisation rate is lowered and the size of the absorbers increases.

At this point, it is important to emphasise that the transmission profiles also vary significantly between individual sight-lines; a strong damping wing will occur whenever there are super-LLS or damped Ly $\alpha$  absorbers lying close to the host halo. This can occur even when the IGM is highly ionised (i.e. for  $\log(\Gamma_{\text{HI}}/\text{s}^{-1}) = -12.8$ ) assuming a sufficiently overdense region lies in close proximity to the LAE. This variation can be seen clearly in Figure 5, which shows the 68 and 95 per cent bounds for the scatter around the median Ly $\alpha$  absorption profile for  $\log(\Gamma_{\text{HI}}/\text{s}^{-1}) = -12.8$  (upper panel) and  $-14.0$  (lower panel). Some Ly $\alpha$  emitters will therefore be completely obscured by the damping wing while others will remain fully visible. The stochastic nature of the damping wing absorption from these high column density systems should therefore also impact on the clustering of LAEs (e.g. Furlanetto et al. 2006; McQuinn et al. 2007a)

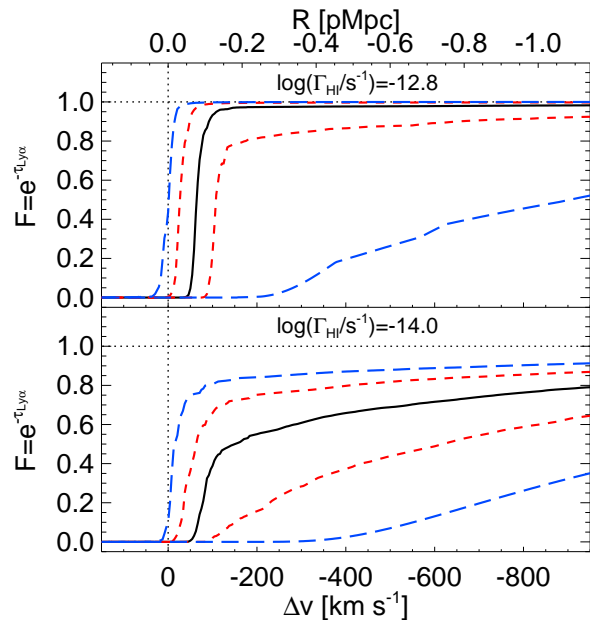


**Figure 5.** The scatter in Ly $\alpha$  transmission along individual sight-lines. Each panel assumes the background photo-ionisation rates indicated on the diagram and include a central ionising source with  $\dot{N}_{\text{ion}} = 1.1 \times 10^{53} \text{ s}^{-1}$ . The short-dashed (red) and long-dashed (blue) curves bound 68 and 95 per cent of the Ly $\alpha$  transmission around the median (black curves). Note the median profiles are identical to those displayed in the central panel of Figure 4.

for even relatively low H I fractions of 3–10 per cent, modifying the enhanced clustering signal expected as the IGM H I fraction rises. This will be an interesting possibility to explore in future work.

In summary, it is clear optically thick absorbers can produce a rapid decline in the transmission of Ly $\alpha$  emission from high-redshift galaxies at the tail-end of reionisation. This is quite different to existing predictions using large-scale numerical and semi-analytical simulations of reionisation. In the late stages of reionisation the presence of self-shielded regions where hydrogen can recombine and stay neutral is very important (Miralda-Escudé et al. 2000; Ciardi et al. 2006; Gnedin & Fan 2006; Choudhury et al. 2009; Crociani et al. 2011; Alvarez & Abel 2012). Large-scale reionisation simulations do not yet have the dynamic range to resolve these systems (see e.g. Trac & Gnedin 2011). Any neutral gas is thus typically far away from the central regions of H II regions, and the impact of nearby optically thick absorbers on the Ly $\alpha$  damping wing is ignored.

We illustrate this in the right-hand panel of Figure 4, where we have simulated the Ly $\alpha$  damping wing expected around a LAE embedded in an H II bubble with radius  $R_{\text{HII}}$ . Inside the bubble ( $R \leq R_{\text{HII}}$ ), the IGM is highly ionised with a uniform H I fraction of  $10^{-4}$ , while outside the IGM is fully neutral. This simple model serves to illustrate the importance of optically thick absorbers for the red damping wing. Bubble sizes of  $R_{\text{HII}} \lesssim 30 \text{ cMpc}$  are required to produce a damping wing similar in strength to the absorption seen when the IGM is only  $\sim 3$  per cent neutral by volume (blue dot-dashed curve in the central panel of Figure 4) when in-

cluding optically thick absorbers. In comparison, large scale reionisation simulations typically predict H I bubble sizes of  $\sim 30\text{--}40$  cMpc for H I fractions as large as 30 per cent (e.g. figure 2 in Zahn et al. 2011). This elucidates why existing models indicate the LAE/LBG fraction at  $z \sim 7$  may imply large H I fractions of 40–90 per cent. At fixed neutral fraction, large-scale reionisation simulations predict a damping wing which is significantly weaker compared to the case where absorption by optically thick absorbers is included. The damping wing will therefore only reduce LAE visibility at times when individual H I bubbles have not yet grown to the typical size of  $\gtrsim 50$  cMpc reached at overlap in these simulations.

### 4.3 The REW distribution

We now compare our models directly to recent measurements of the LBG/LAE fraction (Fontana et al. 2010; Vanzella et al. 2011; Pentericci et al. 2011; Ono et al. 2012; Schenker et al. 2012) following the approach of Dijkstra et al. (2011), which we recapitulate here. Our first requirement is to compute the fraction of the Ly $\alpha$  emission line which is transmitted,  $\mathcal{T}$ , where

$$\mathcal{T} = \frac{\int_{\nu_{\min}}^{\nu_{\max}} d\nu J(\nu) e^{-\tau_{\text{Ly}\alpha}(\nu)}}{\int_{\nu_{\min}}^{\nu_{\max}} d\nu J(\nu)}. \quad (6)$$

Here  $J(\nu)$  gives the shape of the Ly $\alpha$  line profile,  $e^{-\tau_{\text{Ly}\alpha}(\nu)}$  is the IGM transmission (e.g. Figure 4) and  $\nu_{\min}$  and  $\nu_{\max}$  are chosen to correspond to the full extent of our simulated sight-lines. To compute  $\mathcal{T}$  for each of our simulated sight-lines we must assume an intrinsic Ly $\alpha$  profile. We adopt a Gaussian line profile with a standard deviation of  $88 \text{ km s}^{-1}$ , corresponding to the circular velocity of a dark matter halo of mass  $10^{10} M_{\odot}$  at  $z = 7$  (eq. 25 in Barkana & Loeb 2001). We further assume that the line centre is shifted redward of Ly $\alpha$  by  $400 \text{ km s}^{-1}$ ; this offset is typical of Ly $\alpha$  emission lines associated with LBGs at  $z \simeq 2\text{--}3$  (Steidel et al. 2010), and is chosen to mimic the effect of resonant scattering by the (outflowing) gas on the Ly $\alpha$  line visibility (but see our discussion in the next section).

We next construct a probability distribution  $dP(< \log \mathcal{T})/d \log \mathcal{T}$  for each IGM absorption model using our simulations. For Ly $\alpha$  redshifted relative to systemic we assume the observed rest frame equivalent width (REW) at  $z = 6$ , when the hydrogen in Universe is already highly ionised, to be equal to the emitted REW (i.e.  $\mathcal{T}_{z=6} = 1$ ). If we further assume that there is no intrinsic evolution in the LAE population from  $z = 6$  to  $z = 7$ , the cumulative probability distribution (CPDF) that a galaxy has an observed REW and an IGM transmission  $\mathcal{T}$  at  $z = 7$  is

$$P(> \text{REW}) = \int_0^1 d\mathcal{T} \frac{dP(< \log \mathcal{T})}{d \log \mathcal{T}} \frac{P_{z=6}(> \text{REW}/\mathcal{T})}{\mathcal{T} \ln 10}. \quad (7)$$

Here  $\text{REW}_{\text{intr}} = \text{REW}/\mathcal{T}$ ,  $P_{z=6}(> \text{REW}) = \exp(-\text{REW}/\text{REW}_c)$  and  $\text{REW}_c = 50 \text{ \AA}$  (see Dijkstra et al. 2011 for details).

Figure 6 displays the resulting CPDFs for the IGM models with self-shielding only (left panel) and including ionisation by a central LAE (central panel). Note again these two cases have been chosen to bracket the uncertain impact of Lyman continuum emission from the central LAE on the

surrounding IGM (see also the discussion in Section 4.4). The CPDFs are compared to a recent data compilation presented by Ono et al. (2012), as well as an upper limit at  $75 \text{ \AA}$  from Stark et al. (2010). All curves in the central panel lie above the quoted observational uncertainties, implying a lower line-of-sight escape fraction ( $f_{\text{esc}} < 0.2$ ) is required to match the data if the H I fraction remains fixed. As expected, however, our simulations do predict a rapid evolution in the REW distribution from  $z = 6$ , even for modest neutral fractions of 3 per cent (blue dot-dashed curve). In the right panel, the CPDF for the  $\log(\Gamma_{\text{HI}}/\text{s}^{-1}) = -14.0$  model in the central panel (orange long-dashed curve with  $\langle f_{\text{HI}} \rangle_{\text{V}} \sim 0.1$ ) is shown assuming four different offsets for the Ly $\alpha$  emission line relative to systemic. Shifting the line blueward (redward) of the fiducial  $-400 \text{ km s}^{-1}$  decreases (increases)  $\mathcal{T}$ , producing a stronger (weaker) evolution in the REW distribution.

### 4.4 Uncertainties

From our discussion thus far, it should be clear that modelling the IGM transmission for LAEs at the tail-end of reionisation is uncertain mainly because of the difficulties with self-consistently modelling self-shielded regions. However, uncertainties associated with the escape of ionising radiation from the (possibly clustered) Ly $\alpha$  emitters and the redshift relative to systemic of the Ly $\alpha$  emission also play a role.

When including an LAE in our models we have assumed  $f_{\text{esc}} = 0.2$ . It is, however, not obvious that high redshift galaxies emit ionising and Ly $\alpha$  radiation at the same time and/or in the same direction. It is certainly plausible that no ionising radiation escapes in the direction of the observer (e.g. Gnedin et al. 2008), in which case even our IGM model excluding a central source (i.e. the left panel in Figure 6) may actually be an overestimate of the IGM transmission  $\mathcal{T}$ ; recall we have ignored all neutral gas within 20 pkpc of the halo centre and instead assumed the appropriate escape fractions for ionising and Ly $\alpha$  photons. Note further that the escape of ionising radiation and the emission redshift relative to systemic may also be unfavourably coupled. A large redshift for the emission line may need a large column density of neutral gas within the host halo of the LAE. This is required in order to resonantly scatter the Ly $\alpha$  photons locally far into the red wing of the line (e.g. Barnes et al. 2011). The redshifts of  $400 \text{ km s}^{-1}$  or more for the observed Ly $\alpha$  emission in  $z = 3$  LBGs (Steidel et al. 2010) may therefore be incompatible with a simultaneous escape of ionising radiation along the line-of-sight to the observer.

The detailed intrinsic line Ly $\alpha$  shape is also rather uncertain – in this work we have assumed a simple Gaussian line profile with standard deviation  $88 \text{ km s}^{-1}$ . In practice, however, radiative transfer models predict a characteristic double peaked emission line (e.g. Verhamme et al. 2006) with intergalactic Ly $\alpha$  absorption removing the blue peak at high redshift. In their recent analysis of the REW distribution predicted by large-scale reionisation simulations, Jensen et al. (2012) adopt a doubled peaked Gaussian minus a Gaussian line based on the radiative transfer simulations presented by Laursen et al. (2011). They note that using this line profile weakens the impact of the H I fraction on the REW distribution compared to a simple Gaussian

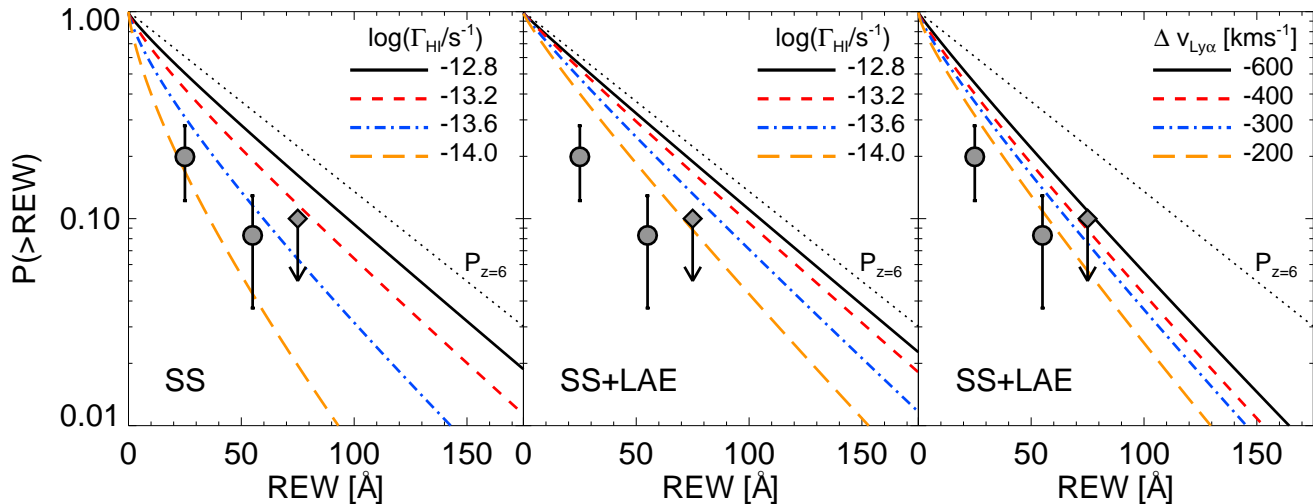


**Figure 6.** Predicted cumulative probability distributions (CPDFs) for the rest frame Ly $\alpha$  equivalent width (REW) at  $z = 7$ . The dotted curves display the intrinsic  $z = 6$  CPDF assuming the IGM is fully transparent to Ly $\alpha$  photons (Dijkstra et al. 2011). The solid, short-dashed, dot-dashed and long-dashed curves are constructed from our Ly $\alpha$  transmission models at  $z = 7$  excluding (left) and including (centre) ionising radiation emitted along the line of sight from a source with  $L_{\text{Ly}\alpha} = 5 \times 10^{42} \text{ erg s}^{-1}$  and  $\dot{N}_{\text{ion}} = 1.1 \times 10^{53} \text{ s}^{-1}$  (see text for details). These models adopt an intrinsic REW distribution identical to that at  $z = 6$  and differ due to evolution in the Ly $\alpha$  transmission only. A Gaussian Ly $\alpha$  profile with a standard deviation of  $88 \text{ km s}^{-1}$  and an offset of  $-400 \text{ km s}^{-1}$  redward of rest frame Ly $\alpha$  has been assumed in both cases. The right hand panel instead displays the  $\log(\Gamma_{\text{HI}}/\text{s}^{-1}) = -14.0$  case from the central panel (with  $\langle f_{\text{HI}} \rangle_{\text{V}} \sim 0.1$ ) assuming four different Ly $\alpha$  emission line offsets. The models are compared to the composite data set compiled by Ono et al. (2012) (filled circles) which utilises observations from Fontana et al. (2010); Vanzella et al. (2011); Pentericci et al. (2011) and Schenker et al. (2012). The upper limit at  $75 \text{ \AA}$  is based on the earlier non-detection by Stark et al. (2010) at  $z \sim 7$ .

centred at the systemic redshift. Note, however, since we adopt a profile which is shifted redward of systemic, our assumption that the entire line is visible in the absence of a red Ly $\alpha$  damping wing is reasonable. Unless the line width becomes comparable to the line offset relative to systemic, this will not have a significant effect on the resulting REW distribution.

Lastly, the small simulation box size of  $10h^{-1} \text{ cMpc}$  and the omission of self-consistent modelling for the ionising sources remains the most significant concern in this analysis. We do not correctly model large-scale variations in the IGM ionisation state prior to overlap. On the other hand, we argue that the proper modelling of dense, self-shielded regions are an equally important part of this problem. A fully self-consistent model will require combining both of these aspects, either by resolving all relevant physical scales or adopting sub-grid models which are informed by high resolution simulations of the IGM density field. Furthermore, any modelling should be calibrated to reproduce the observed transmission redwards of Ly $\alpha$  in bright high-redshift quasars which appears to evolve rapidly between  $z = 6-7$ ; the simulations presented here have been used to estimate a neutral fraction of  $> 10$  per cent around the  $z = 7.085$  quasar ULAS J1120+0641 (e.g. Mortlock et al. 2011; Bolton et al. 2011). Note, however, this is based on a small number of bright quasars at  $z \sim 6$  and only one at  $z > 7$ . Future observations will help determine whether ULAS J1120+0641 is typical.

## 5 CONCLUSIONS

We have used a hydrodynamical simulation to model the Ly $\alpha$  opacity of the intervening IGM during the final stages of reionisation. As the photo-ionisation rate drops the opacity redward of rest-frame Ly $\alpha$  is expected to rise rapidly due to the increasing incidence of optically thick absorption systems. Our results indicate that the bulk of the H I opacity will arise from optically thick systems with column densities  $N_{\text{HI}} \sim 10^{18.5} - 10^{19.5} \text{ cm}^{-2}$ . When including these absorption systems in the simulations, only a moderate rise in the volume averaged neutral fraction is required to significantly reduce the transmission redward of rest-frame Ly $\alpha$ .

This result has an important implication for the interpretation of the recently observed decline in the Ly $\alpha$  emission from high-redshift galaxies at  $z \sim 6-7$  (e.g. Stark et al. 2010; Pentericci et al. 2011; Hayes et al. 2011; Ono et al. 2012; Schenker et al. 2012; Curtis-Lake et al. 2012). We find that these observations do not require a large neutral fraction ( $\sim 40-90$  per cent) in the intervening IGM at  $z = 7$  as previously suggested. Instead, if the rapid decline in the LAE/LBG fraction is further corroborated, it may instead be indicative of the rapid decrease of the mean free path of ionising photons expected at the tail-end of reionisation. Furthermore, as we find the Ly $\alpha$  emission from high-redshift galaxies will be suppressed for volume-averaged neutral fractions of only 3–10 per cent, the patchiness of reionisation may produce a more modest impact on the clustering properties of observable high-redshift LAEs than previously predicted.

Our findings may be particularly relevant for future surveys which plan to use the transmission of Ly $\alpha$  emission and

the clustering properties of LAEs to probe deep into the epoch of reionisation. Detecting these LAEs at  $z > 7$  may well become difficult, even when the IGM is only ten per cent neutral. It may also mean that spectroscopic confirmation of high-redshift candidate galaxies identified with the drop-out technique at  $z > 7$  may become problematic, at least until emission lines other than Ly $\alpha$  can be observed with the James Webb Space Telescope. Finally, extending theoretical predictions beyond the approximate approach adopted in this work is vital. This will ultimately require incorporating small-scale absorption systems into simulations which also model the patchy nature of reionisation on large scales. This remains a considerable but fundamental computational challenge for the current generation of reionisation simulations.

## ACKNOWLEDGMENTS

The hydrodynamical simulation used in this work was performed using the Darwin Supercomputer of the University of Cambridge High Performance Computing Service (<http://www.hpc.cam.ac.uk/>), provided by Dell Inc. using Strategic Research Infrastructure Funding from the Higher Education Funding Council for England. We thank Volker Springel for making GADGET-3 available, and Mark Dijkstra, Zoltan Haiman and Matt McQuinn for helpful comments on the draft manuscript. Figure 1 utilises the cube helix colour scheme introduced by Green (2011). JSB acknowledges the support of an ARC postdoctoral fellowship (DP0984947), and thanks Pratika Dayal and Stuart Wyithe for valuable conversations.

## REFERENCES

- Abel, T., Anninos, P., Zhang, Y., & Norman, M. L. 1997, *New Astronomy*, 2, 181
- Altay, G., Theuns, T., Schaye, J., Crighton, N. H. M., & Dalla Vecchia, C. 2011, *ApJ*, 737, L37
- Alvarez, M. A. & Abel, T. 2012, *ApJ*, 747, 126
- Barkana, R. & Loeb, A. 2001, *Phys. Rep.*, 349, 125
- Barnes, L. A., Haehnelt, M. G., Tescari, E., & Viel, M. 2011, *MNRAS*, 416, 1723
- Becker, G. D., Rauch, M., & Sargent, W. L. W. 2007, *ApJ*, 662, 72
- Bolton, J. S. & Haehnelt, M. G. 2007a, *MNRAS*, 374, 493
- Bolton, J. S. & Haehnelt, M. G. 2007b, *MNRAS*, 382, 325
- Bolton, J. S., Haehnelt, M. G., Warren, S. J., Hewett, P. C., Mortlock, D. J., Venemans, B. P., McMahon, R. G., & Simpson, C. 2011, *MNRAS*, 416, L70
- Calverley, A. P., Becker, G. D., Haehnelt, M. G., & Bolton, J. S. 2011, *MNRAS*, 412, 2543
- Choudhury, T. R., Haehnelt, M. G., & Regan, J. 2009, *MNRAS*, 394, 960
- Ciardi, B., Bolton, J. S., Maselli, A., & Graziani, L. 2012, *MNRAS*, 423, 558
- Ciardi, B., Scannapieco, E., Stoehr, F., Ferrara, A., Iliev, I. T., & Shapiro, P. R. 2006, *MNRAS*, 366, 689
- Crociani, D., Mesinger, A., Moscardini, L., & Furlanetto, S. 2011, *MNRAS*, 411, 289
- Curtis-Lake, E. et al. 2012, *MNRAS*, 422, 1425
- Dayal, P., Maselli, A., & Ferrara, A. 2011, *MNRAS*, 410, 830
- Dijkstra, M., Lidz, A., & Wyithe, J. S. B. 2007, *MNRAS*, 377, 1175
- Dijkstra, M., Mesinger, A., & Wyithe, J. S. B. 2011, *MNRAS*, 414, 2139
- Dijkstra, M. & Wyithe, J. S. B. 2010, *MNRAS*, 408, 352
- Fan, X. et al. 2006, *AJ*, 132, 117
- Finkelstein, S. L. et al., 2012, *ApJ* submitted, arXiv:1206.0735
- Finlator, K., Özel, F., Davé, R., & Oppenheimer, B. D. 2009, *MNRAS*, 400, 1049
- Fontana, A. et al. 2010, *ApJ*, 725, L205
- Forero-Romero, J. E., Yepes, G., Gottlöber, S., & Prada, F. 2012, *MNRAS*, 419, 952
- Furlanetto, S. R. & Oh, S. P. 2005, *MNRAS*, 363, 1031
- Furlanetto, S. R. & Oh, S. P. 2008, *ApJ*, 681, 1
- Furlanetto, S. R., Zaldarriaga, M., & Hernquist, L. 2004, *ApJ*, 613, 1
- Furlanetto, S. R., Zaldarriaga, M., & Hernquist, L. 2006, *MNRAS*, 365, 1012
- Gnedin, N. Y. 2000, *ApJ*, 535, 530
- Gnedin, N. Y. & Fan, X. 2006, *ApJ*, 648, 1
- Gnedin, N. Y., Kravtsov, A. V., & Chen, H.-W. 2008, *ApJ*, 672, 765
- Green, D. A. 2011, *Bulletin of the Astronomical Society of India*, 39, 289
- Haardt, F. & Madau, P. 2001, in *Clusters of Galaxies and the High Redshift Universe Observed in X-rays*, Neumann, D. M. & Tran, J. T. V. ed., astro-ph/0106018
- Haiman, Z. 2002, *ApJ*, 576, L1
- Haiman, Z. & Spaans, M. 1999, *ApJ*, 518, 138
- Hansen, M. & Oh, S. P. 2006, *MNRAS*, 367, 979
- Hayes, M., Schaerer, D., Östlin, G., Mas-Hesse, J. M., Atek, H., & Kunth, D. 2011, *ApJ*, 730, 8
- Hu, E. M., Cowie, L. L., Barger, A. J., Capak, P., Kakazu, Y., & Trouille, L. 2010, *ApJ*, 725, 394
- Iliev, I. T., Mellema, G., Pen, U.-L., Merz, H., Shapiro, P. R., & Alvarez, M. A. 2006, *MNRAS*, 369, 1625
- Jeeson-Daniel, A., Ciardi, B., Maio, U., Pierleoni, M., Dijkstra, M., & Maselli, A. 2012, *MNRAS*, 424, 2193
- Jensen, H., Laursen, P., Mellema, G., Iliev, I. T., Sommer-Larsen, J., & Shapiro, P. R. 2012, *MNRAS* submitted, arXiv:1206.4028
- Kashikawa, N. et al. 2006, *ApJ*, 648, 7
- Katz, N., Weinberg, D. H., Hernquist, L., & Miralda-Escude, J. 1996, *ApJ*, 457, L57
- Kohler, K. & Gnedin, N. Y. 2007, *ApJ*, 655, 685
- Komatsu, E. et al., 2011, *ApJS*, 192, 18
- Kuhlen, M. & Faucher-Giguère, C.-A. 2012, *MNRAS*, 423, 862
- Laursen, P., Sommer-Larsen, J., & Razoumov, A. O. 2011, *ApJ*, 728, 52
- Lawrence, A. 2007, *MNRAS*, 379, 1599
- Leitherer, C. et al. 1999, *ApJS*, 123, 3
- Malhotra, S. & Rhoads, J. E. 2004, *ApJ*, 617, L5
- McGreer, I. D., Mesinger, A., & Fan, X. 2011, *MNRAS*, 415, 3237
- McQuinn, M., Hernquist, L., Zaldarriaga, M., & Dutta, S. 2007a, *MNRAS*, 381, 75
- McQuinn, M., Lidz, A., Zahn, O., Dutta, S., Hernquist, L., & Zaldarriaga, M. 2007b, *MNRAS*, 377, 1043

- McQuinn, M., Lidz, A., Zaldarriaga, M., Hernquist, L., Hopkins, P. F., Dutta, S., & Faucher-Giguère, C.-A. 2009, *ApJ*, 694, 842
- McQuinn, M., Oh, S. P., & Faucher-Giguère, C.-A. 2011, *ApJ*, 743, 82
- Mesinger, A. 2010, *MNRAS*, 407, 1328
- Miralda-Escudé, J., Haehnelt, M., & Rees, M. J. 2000, *ApJ*, 530, 1
- Miralda-Escudé, J. 1998, *ApJ*, 501, 15
- Miralda-Escudé, J. & Rees, M. J. 1998, *ApJ*, 497, 21
- Mortlock, D. J. et al. 2011, *Nature*, 474, 616
- Nagamine, K., Choi, J.-H., & Yajima, H. 2010, *ApJ*, 725, L219
- Ono, Y. et al. 2012, *ApJ*, 744, 83
- Ouchi, M. et al. 2010, *ApJ*, 723, 869
- Pawlik, A. H., Schaye, J., & van Scherpenzeel, E. 2009, *MNRAS*, 394, 1812
- Pentericci, L. et al. 2011, *ApJ*, 743, 132
- Prochaska, J. X., O'Meara, J. M., & Worseck, G. 2010, *ApJ*, 718, 392
- Santos, M. R. 2004, *MNRAS*, 349, 1137
- Schaye, J. 2001, *ApJ*, 559, 507
- Schenker, M. A., Stark, D. P., Ellis, R. S., Robertson, B. E., Dunlop, J. S., McLure, R. J., Kneib, J.-P., & Richard, J. 2012, *ApJ*, 744, 179
- Shull, J. M., Harness, A., Trenti, M., & Smith, B. D. 2012, *ApJ*, 747, 100
- Songaila, A. & Cowie, L. L. 2010, *ApJ*, 721, 1448
- Springel, V. 2005, *MNRAS*, 364, 1105
- Stark, D. P., Ellis, R. S., Chiu, K., Ouchi, M., & Bunker, A. 2010, *MNRAS*, 408, 1628
- Steidel, C. C., Erb, D. K., Shapley, A. E., Pettini, M., Reddy, N., Bogosavljević, M., Rudie, G. C., & Rakic, O. 2010, *ApJ*, 717, 289
- Trac, H. & Cen, R. 2007, *ApJ*, 671, 1
- Trac, H. Y. & Gnedin, N. Y. 2011, *Advanced Science Letters*, 4, 228
- Vanzella, E. et al. 2011, *ApJ*, 730, L35
- Verhamme, A., Schaerer, D., & Maselli, A. 2006, *A&A*, 460, 397
- Wyithe, J. S. B. & Bolton, J. S. 2011, *MNRAS*, 412, 1926
- Wyithe, J. S. B., Bolton, J. S., & Haehnelt, M. G. 2008, *MNRAS*, 383, 691
- Zahn, O., Lidz, A., McQuinn, M., Dutta, S., Hernquist, L., Zaldarriaga, M., & Furlanetto, S. R. 2007, *ApJ*, 654, 12
- Zahn, O., Mesinger, A., McQuinn, M., Trac, H., Cen, R., & Hernquist, L. E. 2011, *MNRAS*, 414, 727
- Zheng, Z., Cen, R., Trac, H., & Miralda-Escudé, J. 2011, *ApJ*, 726, 38
- Zheng, Z. & Miralda-Escudé, J. 2002, *ApJ*, 568, L71